

LA-UR- 75 -'f 04

Title:

ULYSSES SOLAR WIND PLASMA OBSERVATIONS AT HIGH  
SOUTHERLY LATITUDES

Author(s):

J. L. Phillips  
S. J. Bame  
W. C. Feldman  
B. E. Goldstein  
J. T. Gosling  
C. M. Hammond  
D. J. McComas  
M. Neugebauer  
E. E. Scime  
S. I. Suess

Submitted to:

Science  
(REVISED)

**Los Alamos**  
NATIONAL LABORATORY



Los Alamos National Laboratory, an affirmative action/equal opportunity employer, is operated by the University of California for the U.S. Department of Energy under contract W-7405-ENG-36. By acceptance of this article, the publisher recognizes that the U.S. Government retains a nonexclusive, royalty-free license to publish or reproduce the published form of this contribution, or to allow others to do so, for U.S. Government purposes. The Los Alamos National Laboratory requests that the publisher identify this article as work performed under the auspices of the U.S. Department of Energy.

Form No. 836 R5-  
ST 2629 10/81

## Ulysses Solar Wind Plasma Observations at High Southerly Latitudes

J.L. Phillips, S.J. Bame, W.C. Feldman, B.E. Goldstein, J.T. Gosling, C.M. Hammond,  
D.J. McComas, M. Neugebauer, E.E. Scime, and S.T. Suess

Abstract. Ulysses solar wind plasma observations through  $-80.2^\circ$  solar latitude and continuing equatorward to  $-40.10$  are summarized. Recurrent high-speed streams and corotating interaction regions dominated at mid latitudes. The speed of the solar wind was typically  $700$  to  $800 \text{ km s}^{-1}$  poleward of  $-35^\circ$ . Corotating reverse shocks persisted farther south than did forward shocks because of the tilt of the heliomagnetic streamer belt. Sporadic coronal mass ejections were seen as far south as  $-60.5^\circ$ . Proton temperature was higher and the electron strahl was broader at higher latitudes. The high-latitude wind contained compressional, pressure-balanced, and Alfvénic structures.

---

J.L. Phillips, S.J. Bame, W.C. Feldman, J.T. Gosling, C.M. Hammond, and D.J. McComas,  
Space and Atmospheric Sciences Group, MS D466, Los Alamos National Laboratory, Los  
Alamos, NM 87545.

B.E. Goldstein and M. Neugebauer, MS 169-506, Jet Propulsion Laboratory, California Institute  
of Technology, 4800 Oak Grove Drive, Pasadena, CA 91109.

E.E. Scime, Department of Physics, West Virginia University, Morgantown, WV 26506

S.T. Suess, Space Science Laboratory/ES82, NASA Marshall Space Flight Center, Huntsville, AL  
35812.

The solar wind is an ionized gas flowing from the solar corona and consisting primarily of free electrons, protons, and doubly-ionized helium. It has been measured at low solar latitudes for over 30 years. Inferences about the high-latitude solar wind have been drawn using *in situ* in-ecliptic measurements (1) and remote sensing techniques (2). The high-speed (600 to 900 km s<sup>-1</sup>) solar wind flows from coronal holes, while the low-speed (300 to 450 km s<sup>-1</sup>) wind flows from open-field regions above or adjacent to the heliomagnetic streamer belt, a closed magnetic-field region encircling the Sun at the heliomagnetic equator. The nature of the boundaries between sources of fast and slow wind, and the source of medium-speed wind (450 to 600 km s<sup>-1</sup>), are not well understood. As the solar magnetic cycle nears sunspot minimum, the streamer belt has a moderate (-10° to -30°) tilt relative to the solar equator and separates large coronal holes which cover the solar poles. Thus the expected solar wind configuration includes slow wind near the heliomagnetic equator and fast wind near the poles. At intermediate heliographic latitudes, and sometimes at low latitudes, solar rotation and the tilt of the heliomagnetic axis can produce alternating regions of slow and fast wind.

The solar wind plasma experiment onboard the Ulysses spacecraft measured the solar wind throughout the southern hemisphere mission phase using separate ion and electron spectrometers (3). Here we present observations and analysis starting after the outbound Jupiter bow shock crossing on 16 February 1992, at 5.40 astronomical units (AU) from the Sun and -6.4° heliographic latitude, through the peak southerly latitude of -80.2° on 13 September 1994 at 2.29 AU, and continuing through 7 January 1995, when Ulysses reached 1.52 AU and -40.1°.

Wind speed was slow and irregular through June 1992, with little discernible stream pattern (Fig. 1). Beginning in July 1992 a well-defined recurrent high-speed stream was observed, with a location indicating a coronal source at an equatorward extension of the south polar coronal hole (4). This stream was observed fifteen times, recurring every 26 days through early-July 1993. A coronal mass ejection (CME) in November 1992 resulted in instantaneous wind speeds approaching 1000 km s<sup>-1</sup>. The two-decade variations in plasma density resulted from

alternating encounters with coronal-hole and streamer-belt wind and from corotating interaction regions (CIRS), compression regions driven by fast wind overtaking slow wind. In April 1993 the minimum wind speed increased from ~400 to 550 km S-1, roughly coincident with the last encounter with the heliomagnetic current sheet, a magnetic field reversal located within the streamer-belt plasma (4).

Beyond ~2 AU from the Sun the forward and reverse waves bounding CIRS commonly steepened into pairs of fast magnetosonic shocks. CIRS observed by Ulysses at low latitudes were generally bounded by leading forward shocks and trailing reverse shocks. After the spacecraft passed a latitude corresponding to the tilt of the streamer belt (290), only one additional CIR-driven forward shock was observed, whereas the reverse shocks persisted. Furthermore, the forward shocks produced northward flow deflections, while the reverse shocks produced southward deflections. This pattern was interpreted as resulting from equatorward (poleward) propagation of the forward [reverse) shocks, resulting from solar rotation and the tilt of the streamer belt relative to the rotational equator (5). The reverse shocks trailing the CIRS can propagate substantially poleward of the actual interface between fast and slow wind and can influence high-latitude cosmic ray propagation and solar wind particle energization.

In late-July 1993 the minimum wind speed at Ulysses increased again, to ~675 km s-1. Since that time, the spacecraft has been continuously immersed in fast solar wind from the south polar coronal hole (Fig. 2). Evidence for equatorial stream interactions persisted in the Ulysses observations until April 1994. The last reverse shock was observed at -58.2°, with a flow deflection and position in solar longitude indicating a source at the main equatorial CIR (6). After May 1994 the solar-rotation periodicity in wind speed vanished, giving way to an irregular pattern within a speed range of 700 to 800 km S-1. Average speeds increased and variability in density decreased slightly near highest latitudes. Typical values for speed and scaled density near -80° latitude were 770 km S-1 and 2.7 cm<sup>-3</sup>, respectively, similar to those for flows from the broadest coronal holes in the ecliptic plane (7). The continued absence of CIRS and reverse shocks in the

most recent data as the spacecraft returned to mid-latitudes may be due to two factors. First, the orbit is eccentric, with mid-latitudes transited northbound at 1.5 to 2 AU as compared to 4 to 5 AU southbound. The waves bounding CIRs generally do not steepen into shocks until roughly 2 AU. Second, the continued evolution of the Sun toward its sunspot minimum configuration resulted in a decrease in the maximum southerly extent of the heliomagnetic current sheet, as inferred from Wilcox Solar Observatory photospheric field measurements, from  $-25^\circ$  to  $-12^\circ$  during April through September 1994 (8).

One mid-latitude CME supported a scenario of coronal magnetic reconnection behind the ejection, based on a flux-rope magnetic topology observed by Ulysses and on a Yohkoh observation of a long-duration soft x-ray event (9). The last CME observed to date was in April 1994 at  $-60.5^\circ$ . Several CMES were observed at relatively high latitudes, with some unusual properties when compared to in-ecliptic events. All identified high-latitude CMES had speeds comparable to the ambient wind speeds (700 to 800  $\text{km s}^{-1}$ ) (10). All had relative abundances of doubly-charged helium which were similar to or only slightly higher than those in the surrounding wind (-4% of proton abundance), whereas low-latitude CMES often have substantially higher helium abundances. Three distinctive events were identified that had leading forward shocks and trailing reverse shocks driven, not by a speed differential between the ejects and the ambient wind, but rather by expansion caused by high internal pressure (11).

Key solar wind fluid parameters - average speed, density, mass flux, and momentum flux - were highly variable at low latitudes but much less variable poleward of  $-40^\circ$  (Fig. 3). The relatively smooth variation in median wind speed from  $-10^\circ$  to  $-40^\circ$  was due to varying sampling of fast and slow wind, even though the separation between these two wind types was quite distinct. The solar-rotation-averaged maximum speed changed little with latitude poleward of  $-15^\circ$ , while the minimum speed increased in two steps, from  $-400$  to  $-550$  to  $-675$   $\text{km s}^{-1}$ . Mass flux and momentum flux were much more constant than either speed or density as a result of the well-documented negative correlation between the latter two quantities (12). To date there is no clear evidence of substantial differences in prevailing fluid properties during Ulysses' northbound transit

when compared to similar latitudes southbound, except perhaps for a narrower range for all parameters from  $-50^\circ$  to  $-60^\circ$  in the more recent data.

The temperature of the solar wind protons exhibited clear differences between high and low latitudes, similar to in-ecliptic findings of differences between fast and slow wind (Fig. 4). The out-of-ecliptic mission, with its prevailing high-speed wind, had higher temperatures for given heliocentric distances, and a steeper radial gradient, when compared to the in-ecliptic phase with its slow and medium-speed wind. The Ulysses temperatures are consistent with fast-wind and medium-wind values for 1 AU from the IMP mission (7).

A prevailing difference in the character of the solar wind electron distribution functions was observed between low and high latitudes (Fig. 5). The suprathermal anti-sunward field-aligned beam, or *strahl*, which carries most of the electron heat flux from the hot corona to the cold outer heliosphere, was significantly broader in angle at high latitudes than for high-speed flows at low latitudes. This result runs counter to the expectation that the shorter field-aligned path lengths from the corona to the spacecraft at high latitudes should result in less pitch-angle scattering and in narrower electron beams. The high-latitude *strahl* was usually substantially broader in pitch angle than those typically observed in the high-speed wind in the ecliptic plane at 1 AU and in the inner solar system (14). The mechanism for broadening the high-latitude *strahl* is currently unknown. The pronounced Alfvén waves at observed at high latitudes (15) may be a factor, if not through direct interaction with the electron distributions then possibly by lengthening the field-aligned path from the Sun and enabling more collisional scattering. Alternatively, the broadening of the *strahl* may involve nonlinear effects such as turbulence in the inner solar system.

The solar wind at high latitudes exhibited a variety of fine structure; that structure can be characterized as either Alfvénic, pressure-balanced, or compressive. Alfvénic fluctuations were seen as quasi-periodic variations in the non-radial magnetic field and flow components, with periods of one hour or greater and often exceeding ten hours (15). In the pressure-balanced structures, as from 2330 UT on 6 June 1994 through 0430 on 7 June (Fig. 6), plasma pressure and magnetic pressure changed in opposite directions while total pressure remained relatively

constant and plasma beta (the ratio of plasma pressure to magnetic pressure) increased. Structures of this type could be the interplanetary manifestations of polar plumes (16), which are ray-like features in the polar solar corona (17). Competing models for the evolution of plume plasma predict interplanetary signatures that can be either hotter or cooler than the surrounding plasma, but which are always denser (18).

In the compressive structure in Fig. 6, from 1730 UT on 7 June 1994 through 1030 on 8 June, all pressures increased while wind speed was rising, a typical signature of compressions in the solar wind (19). The most intense examples of compressional structure are the CIRs encountered at low and mid-latitudes. As the spacecraft proceeded southward, the CIRs gave way to an irregular series of small-scale compressions (16) (Fig. 7). From  $-23^\circ$  to  $-35^\circ$  there was an obvious solar longitude structure to  $dV/dt$ . From  $-35^\circ$  to  $-62^\circ$  the fit shape was similar but the amplitude was greatly reduced. For the highest-latitude data the fit was essentially flat, indicating that the modulation of  $dV/dt$ , and hence of solar wind compressions, by solar rotation had vanished. This effect may be due to a combination of the increasing southerly latitude of the spacecraft and the simultaneous flattening of the heliomagnetic current sheet (8). The presence of high-latitude compressional features without a solar-rotation ordering suggests that inhomogeneities within the south polar coronal hole itself were the source of these compressions.

#### REFERENCES AND NOTES

1. X.-P. Zhao and A.J. Hundhausen, *J. Geophys. Res.* 86, 5423 (1981); R. Bruno *et al.*, *Solar Phys.* 104,431 (1986).
2. B.J. Rickett and W.A. Coles, *J. Geophys. Res.* 96, 1717 (1991); T. Summanen *et al.*, *J. Geophys. Res.* 98, 13,215 (1993).
3. S.J. Bame *et al.*, *Astron. Astrophys. Supp. Ser.* 92, 237 (1992); Both instruments use spherical section electrostatic analyzers, which direct charged particles into arrays of channel electron multipliers for detection. Stepping of the voltages on the analyzer plates varies the energy-per-charge passbands of the instruments within ranges of 1.6 eV to 862 eV for electrons and 256 eV per charge to 35 keV per charge for positively-charged ions. The multiplier arrays and the 5-

rpm spacecraft spin enable comprehensive look-direction sampling. During the out-of-ecliptic mission, electron spectra were returned every 5.7 to 11.3 minutes and ion spectra were returned every 4.0 to 8.0 minutes. Plasma parameters shown in this study were obtained by numerical integration and functional fitting of the measured particle distribution functions,

4. S.J. Bame *et al.*, *Geophys. Res. Lett.* 20, 2323 (1993); A. Balogh *et al.*, *Geophys. Res. Lett.* 20, 2331 (1993); E.J. Smith *et al.*, *Geophys. Res. Lett.* 20, 232-1 (1993).
5. J.T. Gosling *et al.*, *Geophys. Res. Lett.* 20, 2789 (1993); V.J. Pizzo and J.T. Gosling, *Geophys. Res. Lett.* 21, 2063 (1994), J.T. Gosling *et al.*, *Space Sci. Rev.* 72, 99 (1995).
6. J.L. Phillips *et al.*, *Geophys. Res. Lett.* 21, 1105 (1994); J.L. Phillips *et al.*, *Adv. Space Res.*, in press.
7. W.C. Feldman *et al.*, in *The Solar Output and its Variation*, O.R. White, Ed. (Colorado Associated University Press, Boulder, 1977), pp. 351-382.
8. J.T. Hoeksema, unpublished material. Calculations assumed a radial photospheric field and a source surface at 3.25 solar radii.
9. J.T. Gosling *et al.*, *Geophys. Res. Lett.* 21, 237 (1994); J.T. Gosling *et al.*, *Space Sci. Rev.* 72, 135 (1995).
10. J.T. Gosling *et al.*, *Geophys. Res. Lett.* 21, 1109 (1994).
11. J.T. Gosling *et al.*, *Geophys. Res. Lett.* 21, 2271 (1994).
12. M. Neugebauer and C.W. Snyder, *J. Geophys. Res.* 71, 4469 (1966).
13. J.L. Phillips *et al.*, *Geophys. Res. Lett.* 19, 1239 (1992).
14. W.C. Feldman *et al.*, *Geophys. Res.* 83, 5285 (1978); W.G. Pilipp *et al.*, *J. Geophys. Res.* 92, 1103 (1987).
15. E.J. Smith *et al.*, *Space Sci. Rev.* 72, 165 (1995).
16. D.J. McComas, unpublished material.
17. S. Koutchmy, *Solar Phys.* 51, 399 (1977).
18. M. Velli *et al.*, *Space Sci. Rev.* 70, 391 (1994); Y.-M. Wang, *Astrophys. J.* 3, 435, L153 (1994).
19. J.T. Gosling *et al.*, *J. Geophys. Res.* 77, 5442 (1972).
20. We thank our colleagues at Sandia National Laboratories and Los Alamos National Laboratory for their contributions to the solar wind plasma experiment, R.K. Sakurai and S.J. Kedge for

data reduction support, A. Balogh for the magnetometer observations used in Fig. 6, J.T. Hoeksema for Wilcox Solar Observatory magnetic field observations and calculations, and R.J. Forsyth and N. Il. Sheeley, Jr. for helpful discussions. The support of the Ulysses Project Offices and project scientists at JPL and ESTEC is gratefully acknowledged. Work at LANL was carried out under the auspices of the U.S. Department of Energy with NASA support. Work at the Jet Propulsion Laboratory of the California Institute of Technology was performed under contract to NASA,

#### FIGURE CAPTIONS

Fig. 1. Six-hour-averaged solar wind proton speed (top trace, scale at left) and proton density (scaled to 1 AU; bottom trace, scale at right), observed by the Ulysses solar wind plasma experiment from 16 February 1992 through 31 July 1993. Solid triangles at top mark heliocentric distance: triangles at bottom indicate heliographic latitude in degrees.

Fig. 2. Same as Fig. 1, but for the interval from 1 August 1993 through 7 January 1995, when Ulysses was constantly immersed in the high-speed solar wind, Scales have changed from Fig. 1.

Fig. 3. Median, 5%, and 95% values for solar wind fluid parameters, binned by solar rotation and plotted versus heliographic latitude, for post-Jupiter observations. Mass-weighting of protons and alphas was used for all parameters. Density, mass flux, and momentum flux were scaled to 1 AU by multiplying by  $R^2$  (AU). Time runs from left to right; the vertical trace indicates peak southerly latitude on 13 September 1994.

Fig. 4. Solar-rotation averaged solar wind proton temperature versus heliocentric distance for the entire Ulysses mission through January 7, 1995. The lower branch represents in-ecliptic data, with time running from left to right; the upper branch shows out-of-ecliptic data, with time running from right to left. Prevailing proton temperatures at 1 AU for fast and average solar wind are

marked at left. CMES and shocked plasma have been deleted. This process was problematic during March 1991 due to a complex series of shocks and CMES (13); that interval is not plotted.

Fig. 5. Counts-versus-pitch angle for suprathermal electrons from 55 to 65 eV, showing two spectra in the high-speed wind at  $-15^\circ$  latitude (heavy dots) and  $-80^\circ$  (crosses). Solid traces represent Gaussian fits, yielding full-width-at-half-maximum values of  $56^\circ$  for the low-latitude spectrum and 810 for the high-latitude spectrum.

Fig. 6. 48-hour time series of solar wind speed (top trace, scale at left) and total, plasma, and magnetic pressures (lower traces, labels at left, scale at right) near  $-67^\circ$  heliographic latitude. Vertical traces bound a pressure-balanced structure and a compressions] structure.

Fig. 7. Fourth-order polynomial fits for solar wind  $dV/dt$  versus spacecraft solar longitude. Each curve represents a latitude range, shown in legend. Each latitude range contained 4000 to 7000 hourly-averaged points; points were sorted by solar longitude and then smoothed over roughly one degree.

Table 1. Solar wind milestones for the Ulysses out-of-ecliptic mission through January 7, 1995.

Event	Date	Heliocentric distance (AU)	Heliographic latitude (deg.)
Highest wind speed (990 km s <sup>-1</sup> in CME)	9 Nov. 1992	5.17	-19.9
Last slow wind (V < 450 km s <sup>-1</sup> )	6 Apr. 1993	4.84	-28.3
Last CIR-driven forward shock	29 Jun. 1993	4.58	-33.6
Last medium wind (V < 600 km s <sup>-1</sup> )	25 Jul. 1993	4.49	-35.4
Last CIR-driven reverse shock	3 Apr. 1994	3.34	-58.2
Last coronal mass ejection	21-22 Apr. 1994	3.24	-60.5

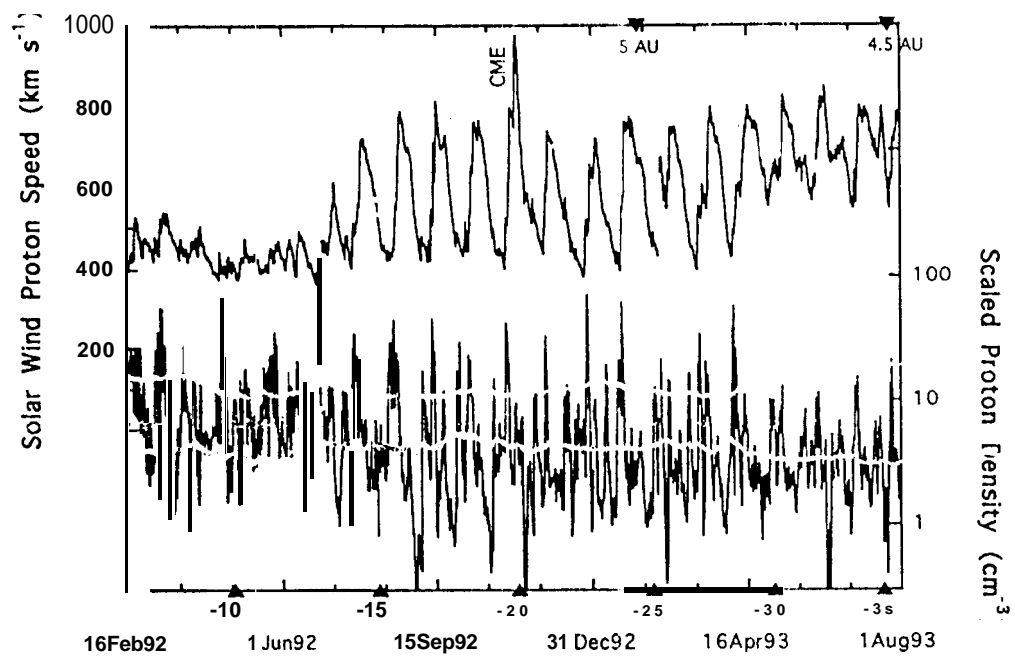


FIG. 1

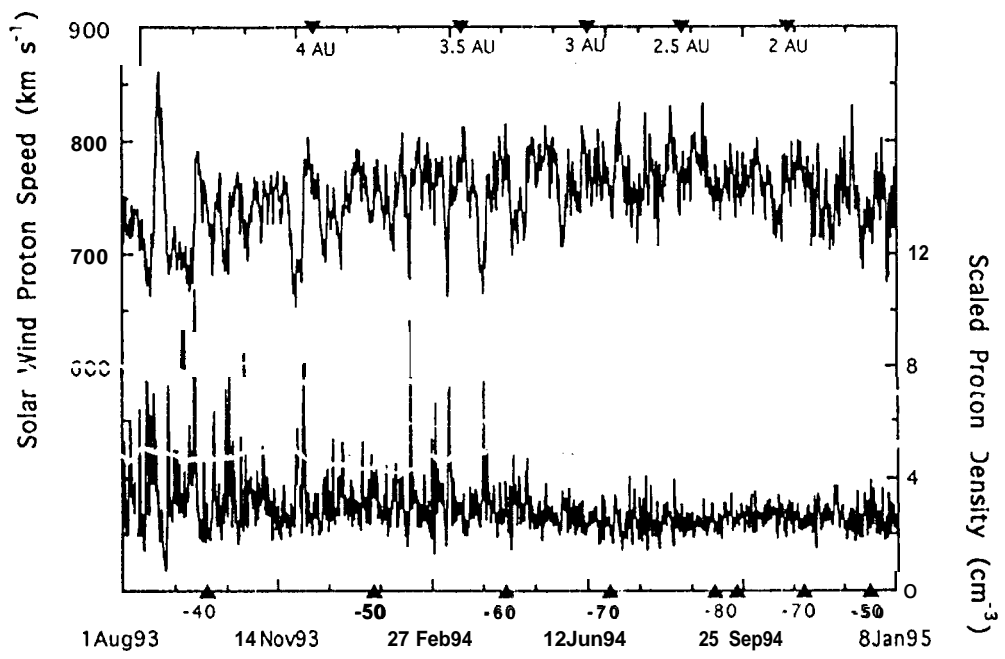
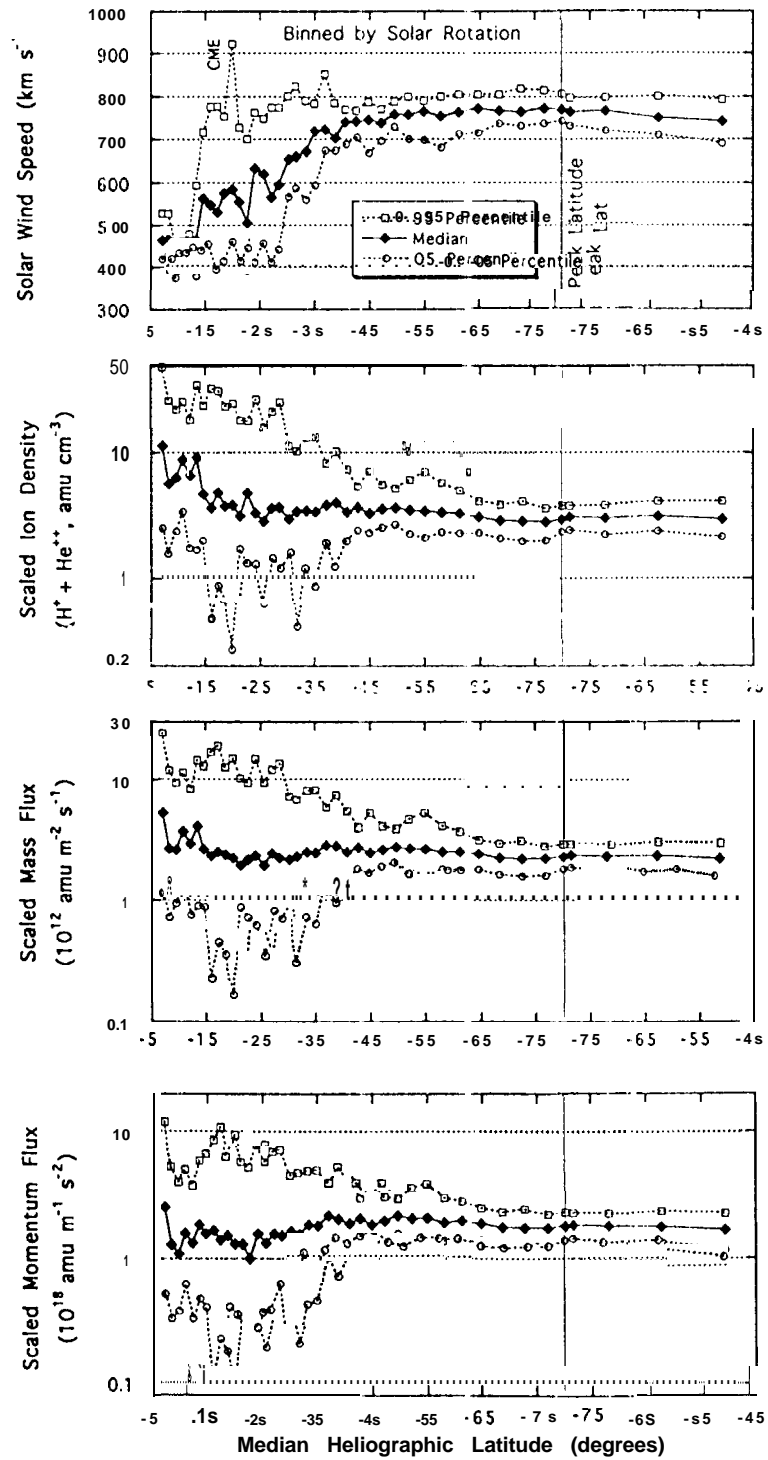


FIG. 2



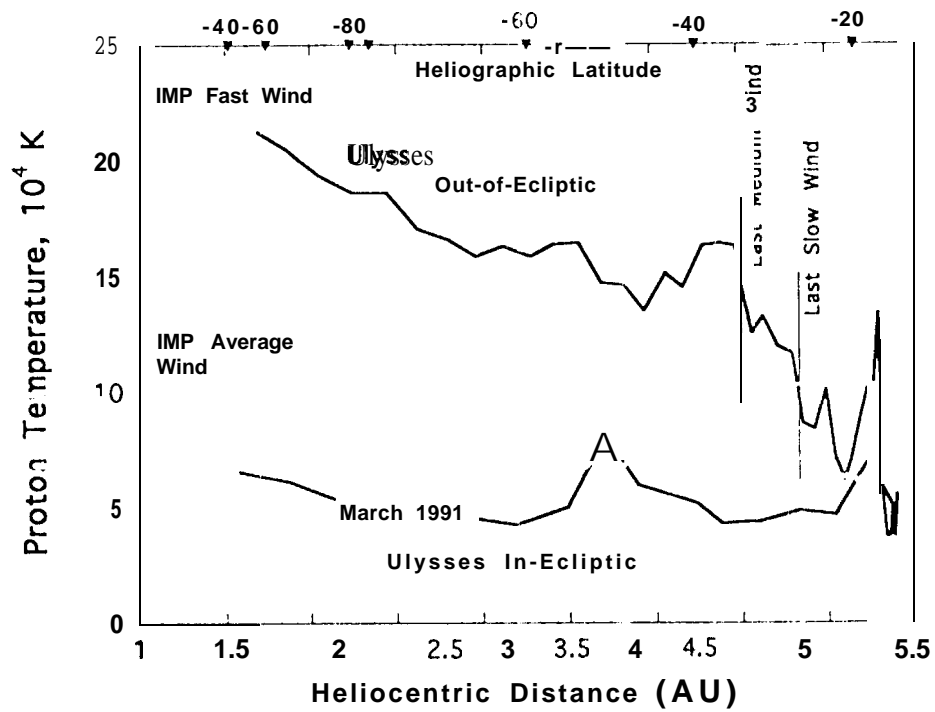


FIG. 4

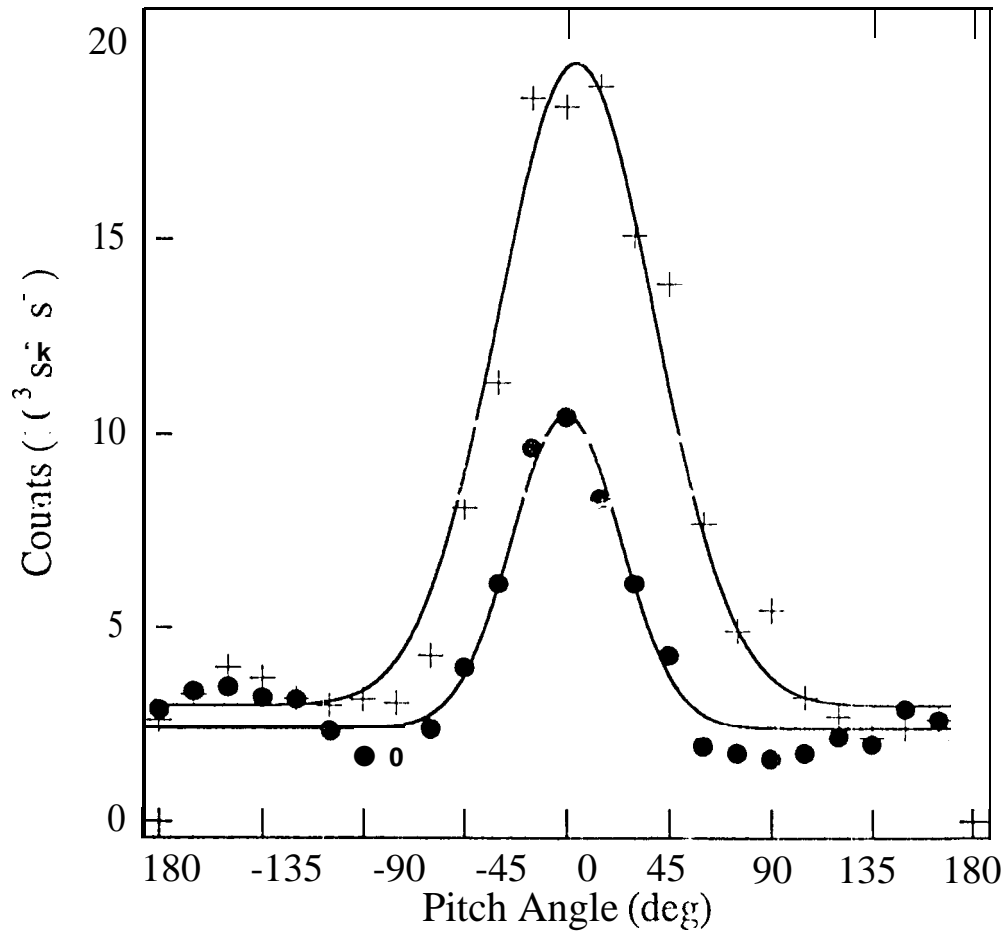


FIG. 5

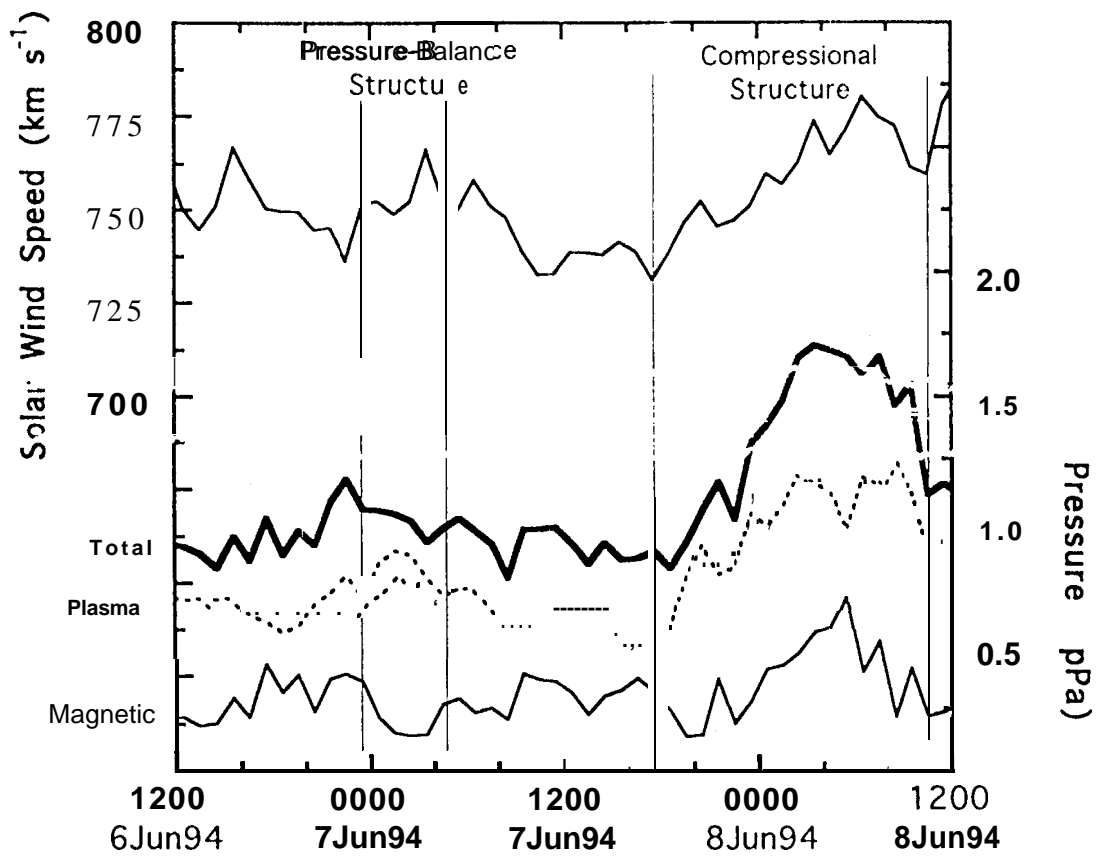


FIG. 6

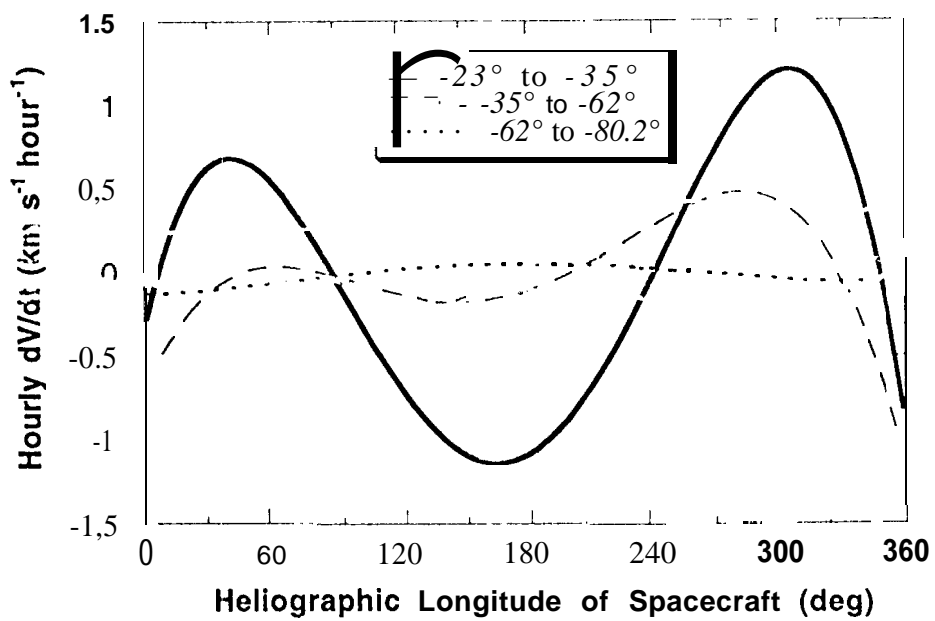


FIG. 7